

Axisymmetric toroidal modes of general relativistic magnetized neutron star models

Hidetaka ASAI

Tohoku University, Sendai, Miyagi 980-8578

hasai@astr.tohoku.ac.jp

and

Umin LEE

Astronomical Institute, Tohoku University, Sendai, Miyagi 980-8578

lee@astr.tohoku.ac.jp

Received _____; accepted _____

Not to appear in Nonlearned J., 45.

ABSTRACT

We calculate axisymmetric toroidal modes of magnetized neutron stars with a solid crust in the general relativistic Cowling approximation. We assume that the interior of the star is threaded by a poloidal magnetic field, which is continuous at the surface with an outside dipole field. We examine the cases of the field strength $B_s \sim 10^{16}$ G at the surface. Since separation of variables is not possible for the oscillations of magnetized stars, we employ finite series expansions for the perturbations using spherical harmonic functions. We find discrete normal toroidal modes of odd parity, but no toroidal modes of even parity are found. The frequencies of the toroidal modes form distinct mode sequences and the frequency in a given mode sequence gradually decreases as the number of radial nodes of the eigenfunction increases. From the frequency spectra computed for neutron stars of different masses, we find that the frequency is almost exactly proportional to B_s and is well represented by a linear function of R/M for a given B_s , where M and R are the mass and radius of the star. The toroidal mode frequencies for $B_s \sim 10^{15}$ G are in the frequency range of the quasi-periodic oscillations (QPOs) detected in the soft-gamma-ray repeaters, but we find that the toroidal normal modes cannot explain all the detected QPO frequencies.

Subject headings: – stars: magnetic field – stars: neutron – stars: oscillations.

1. Introduction

Recent discovery of quasi-periodic oscillations (QPOs) in the decaying tail of the hyper-flares of the three magnetar candidates (hyper-flares from SGR 0526-66 observed in 1979, from SGR 1900+14 in 1998, and from SGR 1806-20 in 2004) has triggered intensive studies of the oscillations of magnetized neutron stars. Observed QPO frequencies are ~ 18 , ~ 30 , and 92.5 Hz for SGR 1806-20 hyperflare (Israel et al. 2005), ~ 28 , 53.5, 84, and 155 Hz for SGR 1900+14 (Strohmayer & Watts 2005). Additional frequencies of 150 and 626 Hz have been identified for SGR 1806-20 (Strohmayer & Watts 2006), and a recent reanalysis for SGR 1806-20 by Hambaryan et al. (2011) indicates QPOs at 16.9, 21.4, 36.8, 59.0, 61.3, and 116.3 Hz. The QPOs are now interpreted as a manifestation of global oscillations of the underlying neutron stars, and it is expected that we will be able to carry out seismological studies of magnetars, neutron stars with an extremely strong magnetic field.

Since the discovery of the QPOs in the magnetar candidates, many researchers have suggested that the QPOs are caused by the oscillations of the underlying neutron star, especially by the crustal torsional modes of the star. For example, it has been suggested that the QPOs are generated by seismic vibrations of the neutron star crust (Israel et al. 2005) and that the QPOs are mainly due to low l fundamental toroidal modes excited in the crust (Strohmayer & Watts 2005, 2006). One of the reasons for such suggestions is that the torsional mode frequencies overlap the observed QPOs and the toroidal crust modes confined in the solid crust might be easily excited by a giant flare, which is probably associated with a restructuring of the magnetic field (Strohmayer & Watts 2006).

Since magnetars are believed to possess an extremely strong magnetic field in the interior, to determine the oscillation frequency spectra of the stars, we need to correctly take account of the effects of the strong magnetic field on the oscillations, that is, we have to calculate not only the crustal toroidal modes modified by the magnetic field, but also the

oscillation modes in the fluid core threaded by the magnetic field. Theoretical calculations of axisymmetric toroidal modes of strongly magnetized neutron stars have so far been carried out by many authors in Newtonian formulation (e.g., Piro 2005; Glampedakis, Samuelsson & Andersson 2006; Levin 2007; Lee 2007, 2008; van Hoven & Levin 2011) and in general relativistic formulation (e.g., Messios et al. 2001; Sotani, Kokkotas & Stergioulas 2007, 2008; Colaiuda & Kokkotas 2011, 2012; Gabler et al. 2011, 2012, 2013; van Hoven & Levin 2012). Since the shear modulus may be dominated by the magnetic pressure in most parts of the crust for a dipole field of strength $B \gtrsim 10^{15}$ G, the crustal toroidal modes are not necessarily well decoupled from the oscillation modes in the fluid core when the core is also threaded by the magnetic field. If the toroidal modes in the crust are strongly coupled with magnetic modes in the core, we have to consider oscillation modes propagating in the entire region of the star. Several authors have calculated such axisymmetric magnetic oscillations using magnetohydrodynamical (MHD) simulations (e.g., Sotani, Kokkotas & Stergioulas 2008, Colaiuda & Kokkotas 2011, 2012; Gabler et al. 2011, 2012, 2013). Most of the authors using MHD simulations to study the oscillations of magnetized stars are able to show the existence of QPOs associated with the edges of the Alfvén continua in the core and are doubtful about the existence of discrete normal toroidal modes in strongly magnetized neutron stars. However, for example, Colaiuda & Kokkotas (2011) have suggested that a crustal toroidal mode can survive as a discrete mode if the frequency is in a gap between the Alfvén continua in the core (see also Levin 2007; van Hoven & Levin 2011). We think it still worthwhile to investigate the oscillations of strongly magnetized neutron stars using a method of calculation different from MHD simulations.

In this paper, we look for axisymmetric normal toroidal modes of magnetized neutron stars with a solid crust using the general relativistic formulation given in Sotani, Kokkotas & Stergioulas (2007). The numerical method to compute normal modes of magnetized neutron stars is the same as that in Lee (2008), who employed series expansions of a finite length

in terms of spherical harmonic functions for the perturbations. We solve two different sets of the oscillation equations, one for fluid regions and the other for a solid crust, and match the solutions at the interfaces between the crust and fluid regions to obtain a complete solution for a mode. We calculate frequency spectra of the axisymmetric toroidal modes of neutron stars threaded by a dipole magnetic field, and compare the computed frequencies with the observed QPO frequencies. §2 describes the method used to construct a neutron star model and a poloidal magnetic field, and the perturbation equations for axisymmetric toroidal modes in magnetized stars are derived in §3. Numerical results are summarized in §4. Discussions are given in §5 and we conclude in §6. The details of the oscillation equations solved in this paper are given in the Appendix. Unless otherwise noted, we adopt units of $c = G = 1$, where c and G denote the speed of light and the gravitational constant, respectively, and the metric signature is $(-, +, +, +)$.

2. Equilibrium configuration

We assume that the neutron star, which is non-rotating and threaded by a dipole magnetic field, is static and spherically symmetric, ignoring the possible deformation of the star due to the magnetic field because the gravitational energy is much larger than the magnetic energy. To calculate neutron star models, we integrate the Tolman-Oppenheimer-Volkoff (TOV) equation using appropriate equations of state, and if we write the line element as

$$ds^2 = g_{\alpha\beta} dx^\alpha dx^\beta = -e^{2\Phi} dt^2 + e^{2\Lambda} dr^2 + r^2 (d\theta^2 + \sin^2 \theta d\phi^2), \quad (1)$$

the functions Φ and Λ satisfy the following equations

$$e^{-2\Lambda} = 1 - \frac{2M_r}{r}, \quad \frac{d\Phi}{dr} = \frac{M_r + 4\pi r^3 p}{r^2 (1 - 2M_r/r)}, \quad (2)$$

where $M_r = \int_0^r 4\pi r^2 \rho dr$ is the gravitational mass, p is the pressure, and ρ is the energy density of the star.

We use the equation of state, for the inner crust and the fluid core, given by Douchin & Haensel (2001), who assume $npe\mu$ matter in the neutron star core, and the equation of state given by Baym, Pethick & Sutherland (1971) for the outer crust. For the fluid ocean we simply use the equation of state for a mixture of a completely degenerate electron gas and a non-degenerate gas of Fe nuclei. For the solid crust, we employ the average shear modulus μ_{eff} (Strohmayer et al. 1991), which in the limit of $\Gamma \equiv (Ze)^2 / (ak_{\text{B}}T) \rightarrow \infty$ is given by

$$\mu_{\text{eff}} = 0.1194 \frac{(Ze)^2 n}{a}, \quad (3)$$

where n is the number density of the nuclei and a is the separation between the nuclei defined by

$$\frac{4\pi}{3} a^3 n = 1, \quad (4)$$

and k_{B} is the Boltzmann constant. We use seven neutron star models, which have different masses and central densities. In Table 1, we summarize the physical properties of the seven neutron star models.

For the magnetic field, we assume an axisymmetric poloidal field produced by a toroidal 4-current J_μ . If we give the 4-current J_μ and the electromagnetic 4-potential A_μ as

$$J_\mu = (0, 0, 0, J_\phi), \quad A_\mu = (0, 0, 0, A_\phi), \quad (5)$$

the Maxwell's equation $F^{\mu\nu}_{;\nu} = 4\pi J^\mu$, where $F_{\mu\nu} = \partial_\mu A_\nu - \partial_\nu A_\mu$, is reduced to

$$e^{-2\Lambda} \frac{\partial^2 A_\phi}{\partial r^2} + \frac{1}{r^2} \frac{\partial^2 A_\phi}{\partial \theta^2} + \left(\frac{d\Phi}{dr} - \frac{d\Lambda}{dr} \right) e^{-2\Lambda} \frac{\partial A_\phi}{\partial r} - \frac{1}{r^2} \frac{\cos \theta}{\sin \theta} \frac{\partial A_\phi}{\partial \theta} = -4\pi J_\phi. \quad (6)$$

Expanding the potential A_ϕ and the current J_ϕ as

$$A_\phi(r, \theta) = a_\ell(r) \sin \theta \frac{\partial}{\partial \theta} P_\ell(\cos \theta), \quad (7)$$

$$J_\phi(r, \theta) = j_\ell(r) \sin \theta \frac{\partial}{\partial \theta} P_\ell(\cos \theta), \quad (8)$$

where $P_\ell(\cos \theta)$ is the Legendre polynomial of order ℓ , we obtain the Grad-Shafranov equation associated with the order ℓ :

$$e^{-2\Lambda} \frac{d^2 a_\ell}{dr^2} + \left(\frac{d\Phi}{dr} - \frac{d\Lambda}{dr} \right) e^{-2\Lambda} \frac{da_\ell}{dr} - \frac{\ell(\ell+1)}{r^2} a_\ell = -4\pi j_\ell. \quad (9)$$

For a dipole field, we use $\ell = 1$, and for the current j_1 , we assume

$$j_1 = f_0 r^2 (\rho + p), \quad (10)$$

where f_0 is an arbitrary constant (Konno et al. 1999). At the centre we may expand the function a_1 as

$$a_1 \approx \alpha_0 r^2 + \mathcal{O}(r^4), \quad (11)$$

where α_0 is another arbitrary constant.

Assuming $j_1^{(\text{ex})} = 0$ for a dipole magnetic field in the exterior region, $a_1^{(\text{ex})}$ is given as

$$a_1^{(\text{ex})} = -\frac{3\mu_b}{8M^3} r^2 \left[\ln \left(1 - \frac{2M}{r} \right) + \frac{2M}{r} + \frac{2M^2}{r^2} \right], \quad (12)$$

where μ_b is the magnetic dipole moment and M is the mass of the star. We determine the constants α_0 and f_0 so that the interior solutions a_1 and da_1/dr are matched with $a_1^{(\text{ex})}$ and $da_1^{(\text{ex})}/dr$ at the surface of the star. The magnetic field $H_\mu = B_\mu/\sqrt{4\pi}$ is then given by

$$H_r = \frac{e^\Lambda \cos \theta}{\sqrt{\pi} r^2} a_1, \quad (13)$$

$$H_\theta = -\frac{e^{-\Lambda} \sin \theta}{\sqrt{4\pi}} \frac{da_1}{dr}, \quad (14)$$

and $H_t = H_\phi = 0$, where $B_\mu = \frac{1}{2} \epsilon_{\mu\nu\alpha\beta} u^\nu F^{\alpha\beta}$. $\epsilon_{\mu\nu\alpha\beta}$ is the completely antisymmetric tensor with $\epsilon_{tr\theta\phi} = \sqrt{-g}$, where g is the determinant of $g_{\mu\nu}$.

3. Method of solution

The stress-energy tensor $T^{\mu\nu}$ for a magnetized neutron star with a solid crust is given by the sum of contributions from a perfect fluid $T_{\text{fluid}}^{\mu\nu}$, a magnetic field $T_{\text{mag}}^{\mu\nu}$ and a shear stress $T_{\text{shear}}^{\mu\nu}$, that is

$$T^{\mu\nu} = T_{\text{fluid}}^{\mu\nu} + T_{\text{mag}}^{\mu\nu} + T_{\text{shear}}^{\mu\nu}, \quad (15)$$

where

$$T_{\text{fluid}}^{\mu\nu} = (\epsilon + p) u^\mu u^\nu + p g^{\mu\nu}, \quad (16)$$

$$T_{\text{mag}}^{\mu\nu} = H^2 u^\mu u^\nu + \frac{1}{2} H^2 g^{\mu\nu} - H^\mu H^\nu, \quad (17)$$

and $\epsilon \equiv \rho$ is the energy density of the matter, $H^2 = H_\mu H^\mu$, and u^μ is the 4-velocity.

The equations of motion for the perturbations are given by the perturbed momentum conservation equation:

$$\delta (h^\mu{}_\alpha T^{\alpha\nu}{}_{;\nu}) = 0, \quad (18)$$

where δ means Eulerian perturbation, and $h^\mu{}_\nu = g^\mu{}_\nu + u^\mu u_\nu$ is the projection tensor, which projects the conservation of the energy-momentum on to the hypersurface normal to u^μ .

The 4-velocity u^μ of the matter in the static equilibrium is given by $u^\mu = (e^{-\Phi}, 0, 0, 0)$.

For axisymmetric toroidal modes, for which we assume $\delta u^t = \delta u^r = \delta u^\theta = 0$ and $\delta\epsilon = \delta p = 0$, equation (18) becomes

$$\begin{aligned} (\epsilon + p + H^2) e^{-\Phi} \frac{\partial}{\partial t} \delta u^\phi &= \delta H^\phi \left[\left(\frac{d\Phi}{dr} + \frac{2}{r} \right) H^r + 2 \frac{\cos \theta}{\sin \theta} H^\theta \right] \\ &+ H^r \frac{\partial}{\partial r} \delta H^\phi + H^\theta \frac{\partial}{\partial \theta} \delta H^\phi - \frac{\partial}{\partial r} \delta T^{r\phi(\text{shear})} - \frac{\partial}{\partial \theta} \delta T^{\theta\phi(\text{shear})} \\ &- \left(\frac{4}{r} + \frac{d\Phi}{dr} + \frac{d\Lambda}{dr} \right) \delta T^{r\phi(\text{shear})} - 3 \frac{\cos \theta}{\sin \theta} \delta T^{\theta\phi(\text{shear})}, \end{aligned} \quad (19)$$

where $\delta u^\phi = e^{-\Phi} \partial \xi^\phi / \partial t$ and ξ^ϕ is the ϕ component of the displacement vector ξ^μ . Here, we have adopted the relativistic Cowling approximation, that is, $\delta g_{\mu\nu} = 0$. According to Schumaker & Thorne (1983), the perturbed shear stress tensors for the toroidal modes are given by

$$\delta T_{r\phi}^{(\text{shear})} = -\mu r^2 \sin^2 \theta \frac{\partial}{\partial r} \xi^\phi(t, r, \theta), \quad (20)$$

$$\delta T_{\theta\phi}^{(\text{shear})} = -\mu r^2 \sin^2 \theta \frac{\partial}{\partial \theta} \xi^\phi(t, r, \theta), \quad (21)$$

where μ is the shear modulus.

Using the Maxwell's equation $F_{[\mu\nu;\gamma]} = 0$ under the ideal MHD approximation, we obtain the relativistic induction equation given by (e.g., Sotani, Kokkotas & Stergioulas 2007)

$$H^\mu{}_{;\nu} u^\nu = -u^\alpha{}_{;\alpha} H^\mu + u^\mu{}_{;\nu} H^\nu + H^\alpha u_{\alpha;\beta} u^\beta u^\mu. \quad (22)$$

Taking Eulerian perturbations of equation (22), we obtain the perturbed induction equation for axisymmetric toroidal modes:

$$e^{-\Phi} \frac{\partial}{\partial t} \delta H^\phi = \frac{d\Phi}{dr} H^r \delta u^\phi + H^r \frac{\partial}{\partial r} \delta u^\phi + H^\theta \frac{\partial}{\partial \theta} \delta u^\phi. \quad (23)$$

Substituting the magnetic field components (13) and (14) and the perturbed shear stress tensors (20) and (21) into equations (19) and (23), we obtain the perturbation equations of axisymmetric toroidal modes of the magnetized neutron stars:

$$\begin{aligned} -e^{-2\Phi} \omega^2 \xi^\phi \left[\epsilon + p + \frac{a_1^2}{\pi r^4} (\cos^2 \theta + \eta \sin^2 \theta) \right] &= \frac{e^{-\Lambda}}{\sqrt{\pi} r^2} \left\{ \left[\left(\frac{d\Phi}{dr} + \frac{2}{r} \right) a_1 \right. \right. \\ &\quad \left. \left. - \frac{da_1}{dr} \right] \cos \theta \delta H^\phi + a_1 \cos \theta \frac{\partial}{\partial r} \delta H^\phi - \frac{1}{2} \frac{da_1}{dr} \sin \theta \frac{\partial}{\partial \theta} \delta H^\phi \right\} + \frac{\partial}{\partial r} \left(\mu e^{-2\Lambda} \frac{\partial}{\partial r} \xi^\phi \right) \\ &\quad + \mu e^{-2\Lambda} \left(\frac{4}{r} + \frac{d\Phi}{dr} + \frac{d\Lambda}{dr} \right) \frac{\partial}{\partial r} \xi^\phi + \frac{\mu}{r^2} \frac{\partial^2}{\partial \theta^2} \xi^\phi + \frac{3\mu \cos \theta}{r^2 \sin \theta} \frac{\partial}{\partial \theta} \xi^\phi, \end{aligned} \quad (24)$$

$$\delta H^\phi = \frac{e^{-\Lambda} \cos \theta}{\sqrt{\pi} r^2} a_1 \frac{\partial}{\partial r} \xi^\phi - \frac{e^{-\Lambda} \sin \theta}{\sqrt{4\pi} r^2} \frac{da_1}{dr} \frac{\partial}{\partial \theta} \xi^\phi, \quad (25)$$

where η is defined by

$$\eta \equiv \frac{1}{4} e^{-2\Lambda} \left(\frac{d \ln a_1}{d \ln r} \right)^2, \quad (26)$$

and we have assumed $\xi^\phi(t, r, \theta) = \xi^\phi(r, \theta) e^{i\omega t}$ and $\delta H^\phi(t, r, \theta) = \delta H^\phi(r, \theta) e^{i\omega t}$.

For the perturbations of magnetized stars the separation of variables between r and (θ, ϕ) is impossible, so we employ finite series expansions of the axisymmetric perturbations in terms of the spherical harmonic functions $Y_l^m(\theta, \phi)$, that is,

$$\xi^\phi(r, \theta) = \sum_{j=1}^{j_{\max}} T_{l'_j}(r) \frac{1}{\sin \theta} \frac{\partial}{\partial \theta} Y_{l'_j}^{m=0}(\theta, \phi), \quad (27)$$

$$\delta H^\phi(r, \theta) = \sum_{j=1}^{j_{\max}} b_{l_j}(r) \frac{1}{\sin \theta} \frac{\partial}{\partial \theta} Y_{l_j}^{m=0}(\theta, \phi), \quad (28)$$

where $l_j = 2j$ and $l'_j = l_j - 1$ for even modes, and $l_j = 2j - 1$ and $l'_j = l_j + 1$ for odd modes for $j = 1, 2, 3, \dots, j_{\max}$ (Lee 2008). Most of the numerical results shown below are obtained for $j_{\max} = 15$. In this convention, the angular pattern of δH^ϕ (of ξ^ϕ) at the stellar surface is symmetric (antisymmetric) about the equator for even modes and it is antisymmetric (symmetric) for odd modes. Note that when the displacement vector is given as the sum of the spheroidal component and toroidal component (e.g., Unno et al 1989), the two components are decoupled for axisymmetric modes of non-rotating stars magnetized with a dipole field as given by equations (27) and (28), and they are coupled for non-axisymmetric modes (e.g., Lee 2007), and that for rotating stars the two components are always coupled for both axisymmetric and non-axisymmetric modes. Substituting the expansions into the perturbed equations, we obtain a set of linear ordinary differential equations, which is formally written as

$$r \frac{d}{dr} \mathbf{Y} = \mathbf{C} \mathbf{Y}, \quad (29)$$

where

$$\mathbf{Y} = \begin{pmatrix} \mathbf{t} \\ \mathbf{h} \end{pmatrix}, \quad (30)$$

and \mathbf{C} is the coefficient matrix, and $\mathbf{t} = (T_{l_j}')_j$ and $\mathbf{h} = (h_{l_j})_j$ with $h_{l_j} = r^3 b_{l_j} / (\sqrt{\pi} a_1)$. Note that the coefficient matrix \mathbf{C} and the dependent vector \mathbf{Y} are defined differently in the fluid and solid regions. See the Appendix for the detail.

The set of ordinary differential equations may be solved as an eigenvalue problem of ω by applying boundary conditions at the center and surface of the star and jump conditions at the core-crust and crust-ocean interfaces. For the inner boundary condition, we require that the functions \mathbf{t} and \mathbf{h} are regular at the center. The outer boundary conditions are given by $\mathbf{h} = 0$, which means that the magnetic traction vanishes at the surface of the star (e.g., Saio & Gautschy 2004; Lee 2005, 2007, 2008). The jump conditions are given by the continuity of the function \mathbf{t} and that of the traction at the two interfaces (e.g., Lee 2007, 2008). In addition we adopt normalization condition $T_1(R) = 1$ for even modes, and $T_2(R) = 1$ for odd modes at the stellar surface.

With the method of calculation we employ for the oscillations of magnetized stars, we find numerous solutions to the oscillation equations for a given $B_S \equiv \mu_b/R^3$. Most of the solutions, however, are dependent on j_{\max} , and we have to look for the solutions that are independent of j_{\max} .

4. Numerical results

4.1. Code test

In order to test our numerical code, we take the Newton limit ($p/\rho c^2 \rightarrow 0$, $\Lambda \rightarrow 0$, and $\Phi \rightarrow 0$) in the oscillation equations, and we replace the inner poloidal field with a dipole

magnetic field of Ferraro (1954) type. The Ferraro type field in Newtonian gravity is given by

$$B_r = \frac{1}{r^2 \sin \theta} \frac{\partial U}{\partial \theta}, \quad B_\theta = -\frac{1}{r \sin \theta} \frac{\partial U}{\partial r}, \quad (31)$$

where U is a scalar function given by $U = (C_1 r^2 + C_2 r^4) \sin^2 \theta \equiv F(r) \sin^2 \theta$ that satisfies the Grad-Shafranov equation for uniform density stars, and C_1 and C_2 are constants to be determined by the boundary conditions. We replace $a_1(r)$ in equations (13) and (14) with the function $F(r)$ for the field of Ferraro type. This replacement makes the oscillation equations the same as those solved by Lee (2008) for axisymmetric toroidal modes of magnetized neutron stars with a solid crust in Newtonian gravity. The results of the axisymmetric toroidal mode calculations for this magnetic field are the same as those in Lee (2008), that is, we find both even and odd modes, and the eigenfrequencies form mode sequences and the frequency in a mode sequence gradually increases as the number of radial nodes of the eigenfunction increases.

4.2. General relativistic calculation

In Figure 1, the oscillation frequencies of the toroidal modes of odd parity of NS08 (left panels) and NS14 (right panels) are plotted versus the number of radial nodes of the eigenfunction $T_{l'}$ for $B_S = 10^{16}$ G (top panels) and $B_S = 5 \times 10^{15}$ G (bottom panels). Note that no toroidal modes of even parity are found in the present calculation. The qualitative property of the frequency spectra obtained for the seven models in Table 1 are almost the same, although as the neutron star mass decreases, the mode frequencies becomes higher, the tendency of which is the same as that found by Lee (2008). Except for the lowest frequency modes, the oscillation frequencies seem to make one parameter mode sequences, and the oscillation frequency in a mode sequence O_1 (or O_2) tends to gradually decrease as the number of radial nodes increase. This tendency of the oscillation frequency in a

mode sequence is different from that found by Lee (2008). In the lowest frequency group indicated by O_0 , we find only three modes, which all have no radial nodes of the function $T_{l'}$. Note that in Figure 1, the three modes in O_0 are not clearly discerned because their frequencies are close to each other. The properties of the oscillation spectrum obtained here are not necessarily the same as those found by Lee (2008), who used the Newtonian gravity and the Ferraro type dipole magnetic field in the interior (see §4.1). The normalized frequencies $\bar{\omega} \equiv \omega/\omega_0$ with $\omega_0 = \sqrt{M/R^3}$ obtained in the present calculation are larger than those of Lee (2008) and the frequency separations between the consecutive mode sequences are wider than those of Lee (2008). In Table 2, we summarize the eigenfrequencies $\bar{\omega}$ of axisymmetric toroidal modes of NS08 and of NS14 for $B_S = 10^{16}$ G.

From Figure 1, we also find that the qualitative behavior of the frequency spectra for $B_S = 5 \times 10^{15}$ G is the same as that for 10^{16} G, although the frequency of the modes, proportional to B_S , is smaller than that for $B_S = 10^{16}$ G. This suggests that the modes we obtain here are essentially Alfvén modes. The number of discrete toroidal modes we can find for $B_S = 5 \times 10^{15}$ G is decreased compared with the case of 10^{16} G, and as B_S becomes further weaker, it becomes more and more difficult to obtain well converged discrete toroidal modes. As suggested by Lee (2008), this difficulty may be caused by the existence of a dense spectrum of core magnetic modes in the frequency range of the crustal modes for a weak field B_S .

In Figure 2, we plot the eigenfunctions of the three toroidal modes in the lowest frequency group O_0 of NS14. We find that the eigenfunctions \mathbf{t} of the three modes look similar, that is, they all have large amplitudes only in the outer envelope, in which the solid crust resides, and have negligible amplitudes in the core. This property is different from that of the toroidal modes belonging to the mode sequences O_1 and O_2 with higher frequencies. As shown by Figure 3, the eigenfunctions \mathbf{t} of the modes in the sequences O_1

and O_2 have large amplitudes only in the fluid core and negligible amplitudes in the crust region.

Figure 4 shows the frequency spectrum of axisymmetric toroidal modes for the case of $B_S = 10^{16}$ G, where we have treated the entire interior of the stars as a fluid, neglecting the solidity of the crust. We find only the toroidal modes of odd parity and no toroidal modes of even parity are found. Many low frequency toroidal modes are found and they form the mode sequence O_0 such that the frequency is ordered according to the number of radial nodes of the function T_l' . Note that the oscillation frequencies of the toroidal modes found for the fluid star are almost the same as those for the star with a solid crust, suggesting that the magnetic field is essential to determine the modal properties of the toroidal modes. For the fluid star, the eigenfunctions \mathbf{t} of the toroidal modes in the sequences O_0 , O_1 , and O_2 have large amplitudes in the core but negligible amplitudes in the envelope, the properties of which are the same as those found in Figure 3. In other words, only the toroidal modes in the O_0 sequence for the models with a solid crust have the distinct eigenfunctions. It is important to note that the frequencies of the toroidal modes for the fluid star are almost exactly proportional to B_S , and we can find discrete toroidal modes even for a magnetic field as weak as $B_S \lesssim 10^{14}$ G.

We may look for higher frequency toroidal modes that form mode sequences such as O_3 , O_4 , and \dots , but we find it very difficult to obtain such high frequency modes, particularly when the number of radial nodes of the eigenfunctions is increased. Because of the difficulty, we are not sure about whether or not we can always find toroidal normal modes of arbitrarily high frequencies.

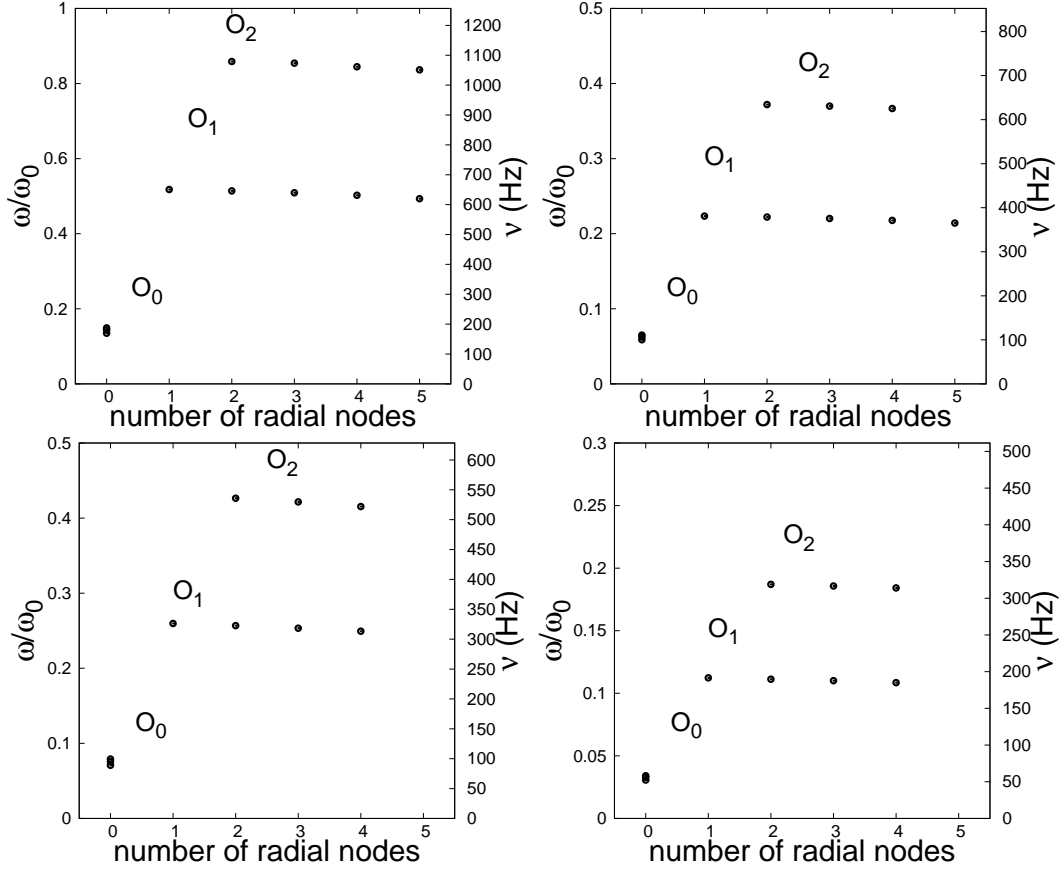


Fig. 1.— Frequencies ω of axisymmetric toroidal modes of NS08 (left panels) and of NS14 (right panels) versus the number of radial nodes of $T_{l'}$, where B_S is 10^{16} G (top panels) and 5×10^{15} G (bottom panels). Here, $\nu = \omega/2\pi$ and $\omega_0 = \sqrt{M/R^3}$ with M and R being the gravitational mass and radius of the star.

Table 1: The main properties of seven neutron star models

Model	M/M_\odot	R (km)	ρ_c (g cm $^{-3}$)	crust thickness (km)	R/M
NS05	0.499	12.235	4.771×10^{14}	3.102	16.584
NS08	0.799	11.940	6.260×10^{14}	1.887	10.111
NS10	0.999	11.882	7.303×10^{14}	1.449	8.042
NS12	1.198	11.823	8.446×10^{14}	1.151	6.680
NS14	1.394	11.729	9.788×10^{14}	0.916	5.693
NS16	1.599	11.564	1.159×10^{15}	0.722	4.896
NS18	1.797	11.284	1.419×10^{15}	0.551	4.249

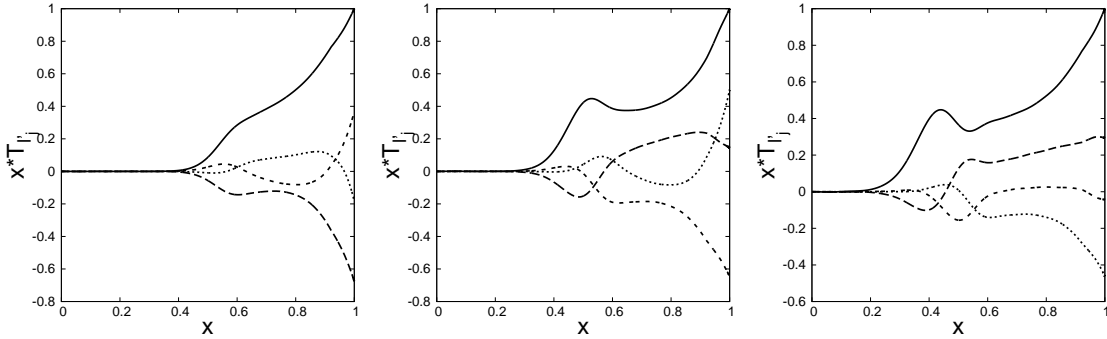


Fig. 2.— Expansion coefficients $xT_{l'}$ as a function of $x = r/R$ for the axisymmetric toroidal modes of odd parity in the O_0 sequence of the model NS14 for $B_S = 10^{16}$ G, where the solid, long-dashed, short-dashed and dotted lines are for the expansion coefficients associated with l'_j from $j = 1$ to 4. Here, the frequency $\bar{\omega} \equiv \omega/\omega_0$ of the modes is, from left to right, 0.05875, 0.06268, and 0.06493, respectively.

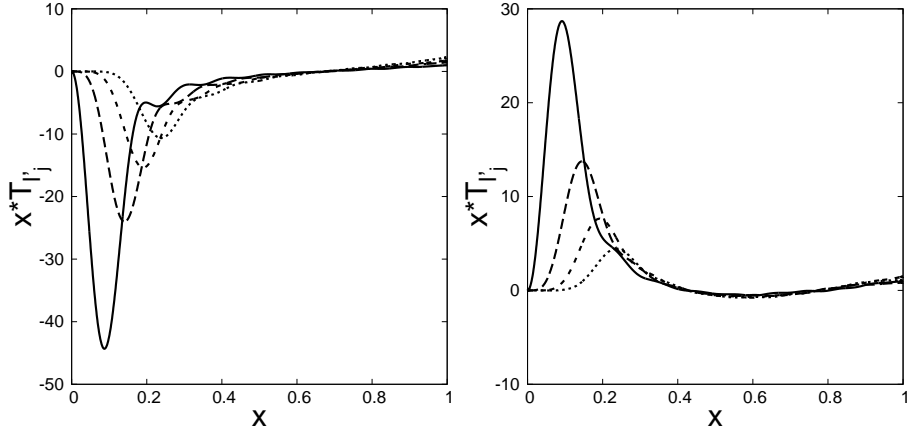


Fig. 3.— Same as Figure 2 but for the toroidal modes in the mode sequences O_1 (left panel) and O_2 (right panel), where the modes have the least number of radial nodes of the eigenfunction $T_{l'}$ in each of the mode sequences. The normalized frequency $\bar{\omega}$ is 0.2235 (left panel) and 0.3720 (right panel).

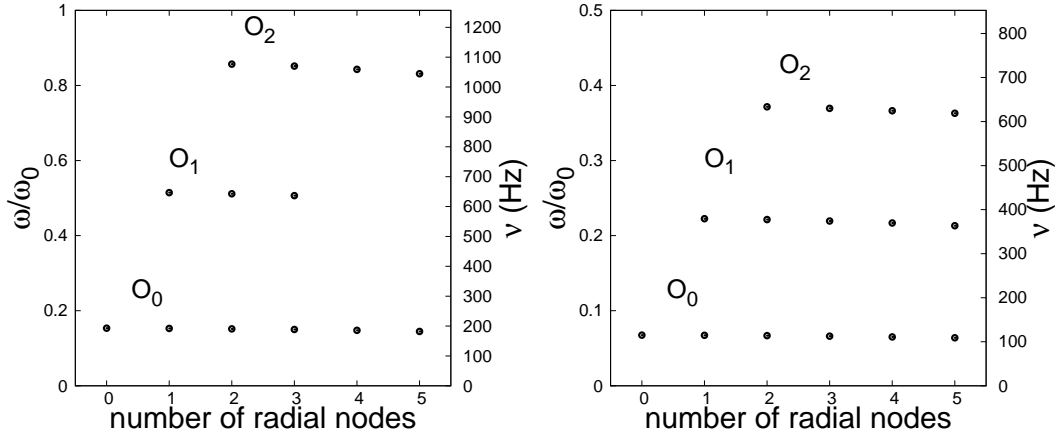


Fig. 4.— Frequencies ω of the axisymmetric toroidal modes of NS08 (left panel) and NS14 (right panel) versus the number of radial nodes of the expansion coefficient $T_{l'}$ for $B_S = 10^{16}$ G. The modes are calculated by treating the entire interior as a fluid.

Table 2: Eigenfrequency $\bar{\omega}$ of the axisymmetric toroidal modes for $B_S = 10^{16}$ G

NS08						
sequence	number of radial nodes					
	0	1	2	3	4	5
$O_0 \dots\dots$	0.1351					
	0.1440					
	0.1492					
$O_1 \dots\dots$		0.5186	0.5148	0.5106	0.5047	0.4970
$O_2 \dots\dots$			0.8593	0.8543	0.8469	0.8366
NS14						
sequence	number of radial nodes					
	0	1	2	3	4	5
$O_0 \dots\dots$	0.0588					
	0.0627					
	0.0649					
$O_1 \dots\dots$		0.2235	0.2221	0.2203	0.2177	0.2142
$O_2 \dots\dots$			0.3720	0.3699	0.3668	

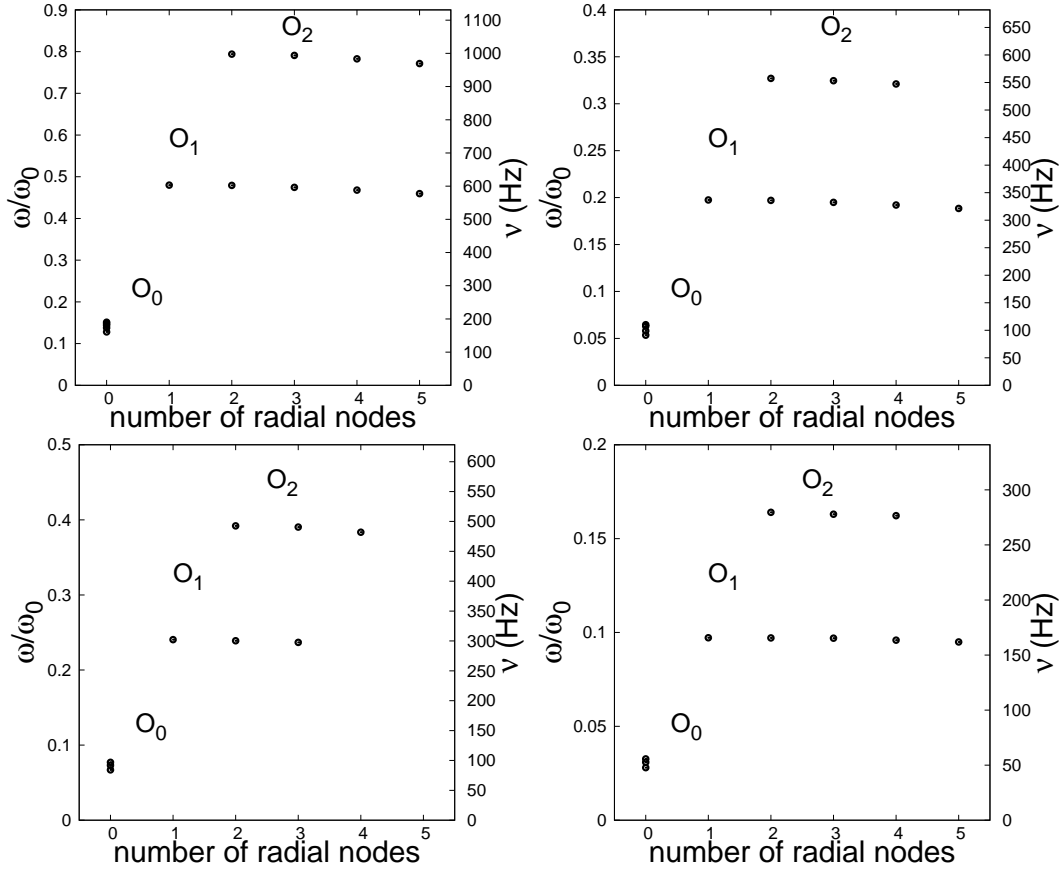


Fig. 5.— Same as Figure 1 but for that the toroidal modes are calculated in the non-relativistic limit of the governing equations. See the text for the detail.

4.3. Newton limit

Let us consider the Newton limit of the present calculations in order to see how the general relativity affects the properties of the oscillation modes. The perturbation equations in the Newton limit may be obtained by assuming $p/\rho c^2 \rightarrow 0$, $\Lambda \rightarrow 0$, and $\Phi \rightarrow 0$ in equations (24) and (25). We also take the Newton limit in the Grad-Shafranov equation for the function a_1 . Figure 5 shows the results for the axisymmetric toroidal modes of NS08 (left panels) and NS14 (right panels) in the Newton limit. Although the frequencies $\bar{\omega}$ are smaller, about by 10%, than those obtained in the relativistic calculation, the qualitative properties of the frequency spectrum remain the same between the two calculations. We also confirm that the eigenfunctions are almost the same as those found in the general relativistic calculation.

5. Discussion

5.1. spatial oscillation pattern

It is useful to examine the spatial oscillation pattern $\hat{\xi}_\phi(r, \theta)$ for the axisymmetric toroidal modes, where $\hat{\xi}_\phi(r, \theta) \equiv r \sin \theta \xi^\phi(r, \theta) = \sum_{j=1}^{j_{\max}} r T_{l'_j}(r) \partial_\theta Y_{l'_j}^0(\theta, \phi)$ and we use $j_{\max} = 15$. Figure 6 shows the pattern $\hat{\xi}_\phi(r, \theta)$ in the $(x = r \cos \theta, y = r \sin \theta)$ plane for the three modes of odd parity in the mode sequence O_0 of the model NS14 for $B_s = 10^{16}$ G (see Figure 1), where the magnetic axis is the horizontal axis given by $y = 0$ and the oscillation amplitudes are normalized by the maximum value. Note that these three modes have no radial nodes of $T_{l'_j}$. From Figure 6, we find that the oscillation pattern is antisymmetric about the equator given by $x = 0$, and that the surface fluid ocean above the solid crust manifests itself as a wavy pattern along the semicircle of $(x^2 + y^2)/R^2 \cong 1$. We also find that the oscillation patterns have large amplitudes surrounding the region of

closed magnetic fields in the model and the number of nodal lines, given by $\hat{\xi}_\phi(r, \theta) = 0$, in the pattern increases with the oscillation frequency, which clearly provides the way of classifying the modes. It is interesting to note that the oscillation patterns associated with the closed magnetic fields obtained by Cerda-Duran et al. (2009), who ignored the solid crust and applied the outer boundary conditions given by $d\mathbf{t}/dr = 0$, have large amplitudes only in the region of the closed fields, although the patterns obtained in this paper have amplitudes in the regions surrounding the closed fields.

In Figure 7, we plot the pattern $\hat{\xi}_\phi(r, \theta)$ for the modes belonging to the sequences O_1 and O_2 in Figure 1, where only the mode with the least number of radial nodes of T_{l_1} is shown for each of the mode sequences. From Figure 7, we find the oscillation patterns have large amplitudes in the narrow regions ($0 \lesssim y/R \lesssim 0.3$) parallel to the magnetic axis ($y = 0$). We also find a wavy pattern along the surface fluid ocean, particularly for the mode in O_2 . The oscillation patterns are quite similar to those given by Cerda-Duran et al. (2009). Note that although only odd parity modes are found in this paper, Cerda-Duran et al. (2009) found both even and odd parity modes.

Figure 8 shows the oscillation patterns of the toroidal modes of odd parity calculated by treating the entire interior as a fluid, where the modes of the least number of radial nodes of T_{l_1} in each of the mode sequences O_0 , O_1 , and O_2 are shown. The oscillation patterns of the modes in the sequences O_1 and O_2 look quite the same between the models with and without the solid crust. However, the patterns of the modes in the sequence O_0 are significantly different between the two cases. For the model without a solid crust, we find only the modes that have large amplitudes along the magnetic axis. No modes are found that have dominant amplitudes in the regions surrounding the closed magnetic fields. We note that the number of nodal lines of $\hat{\xi}_\phi(r, \theta) = 0$ in the (x, y) plane increases with the mode frequency.

It is confirmed that both the eigenfrequency and eigenfunction of the toroidal modes do not change even if we double the number of radial mesh points in the model, where we usually use neutron star models having about 1000 mesh points. Note that the eigenfunctions we obtain for the toroidal modes have no indications of discontinuities in the derivative $d\mathbf{t}/dr$. It is also confirmed that the oscillation patterns as given in Figures 6 to 8 show a good convergence for $j_{\max} \gtrsim 10$.

5.2. dependence on the compactness

To see the dependence of the mode frequency on the compactness of the models, we plot in Figure 9 the oscillation frequency ν of three toroidal modes as a function of the ratio $z \equiv R/M$ for $B_S = 10^{16}$ G, where the modes, which belong to the sequences O_0 , O_1 , and O_2 and have the least number of nodes in each of the sequences, are calculated for the NS models tabulated in Table 1. Applying a least-square fit to the frequency ν of the mode, for example, in the sequence O_0 , we obtain a fitting formula, which is in a good approximation given by a linear function of the parameter z for a given B_S . Since the toroidal mode frequency is almost exactly proportional to B_S in the range of B_S we examined, we can write the oscillation frequency as

$$\nu(z, y) \simeq (c_0 + c_1 z) y, \quad (32)$$

where $y = B_S/(10^{16} \text{ G})$. In Table 3, the coefficients c_0 and c_1 are tabulated for the first three modes in each of the mode sequences O_0 , O_1 , and O_2 . We have also carried out the same calculations by replacing the DH EOS in the core with the APR EOS (Akmal, Pandharipande & Ravenhall 1998), and we obtain quite similar frequency spectra of axisymmetric toroidal modes, and the coefficients c_0 and c_1 have also similar values to those computed for the DH EOS.

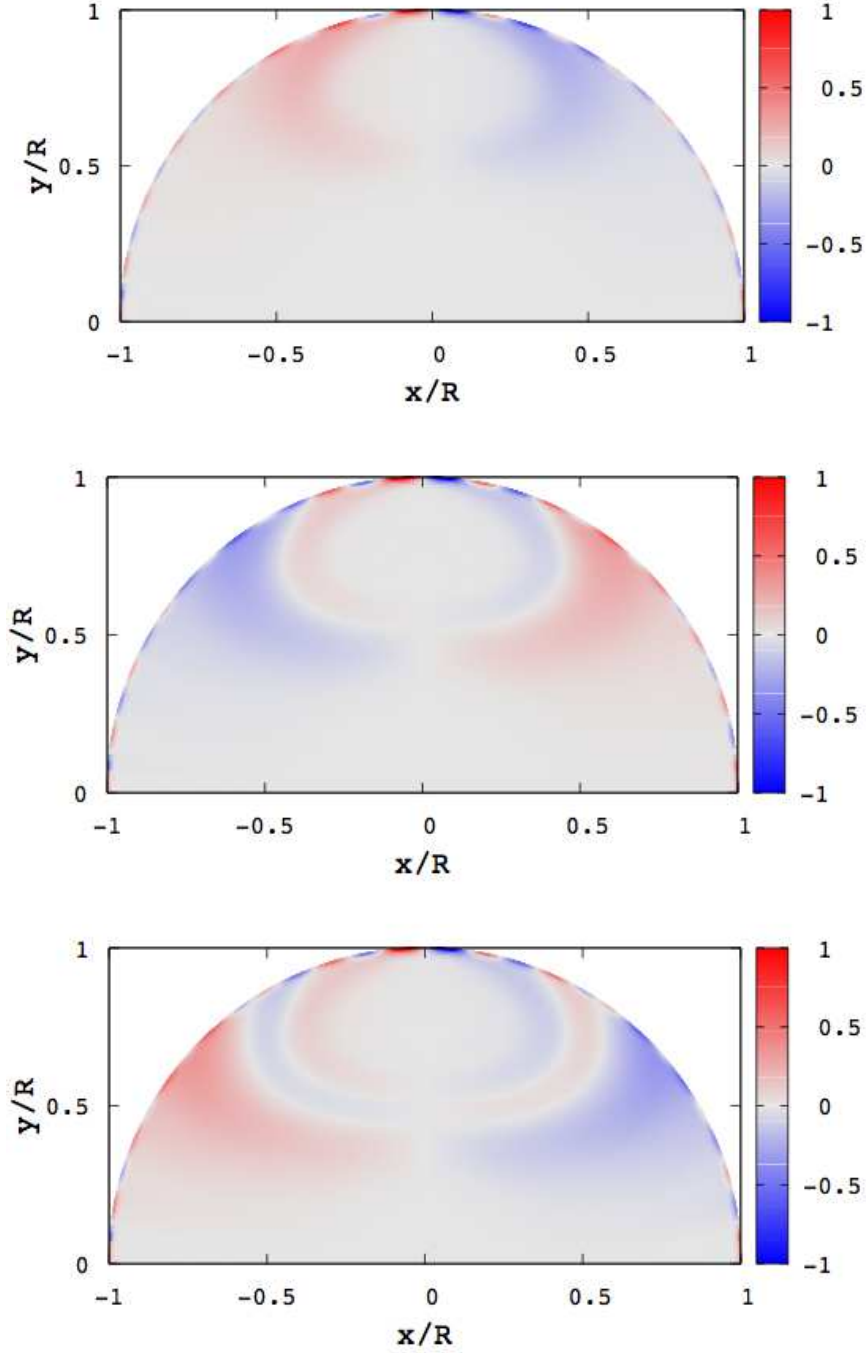


Fig. 6.— Spatial oscillation patterns $\hat{\xi}_\phi(r, \theta)$ of the axisymmetric toroidal modes of odd parity for the model NS14 for $B_S = 10^{16}$ G, where the frequency $\bar{\omega}$ of the modes is, from top to bottom panels, 0.05875, 0.06268, and 0.06493, respectively. These three modes belong to the lowest frequency group O_0 in Figure 1.

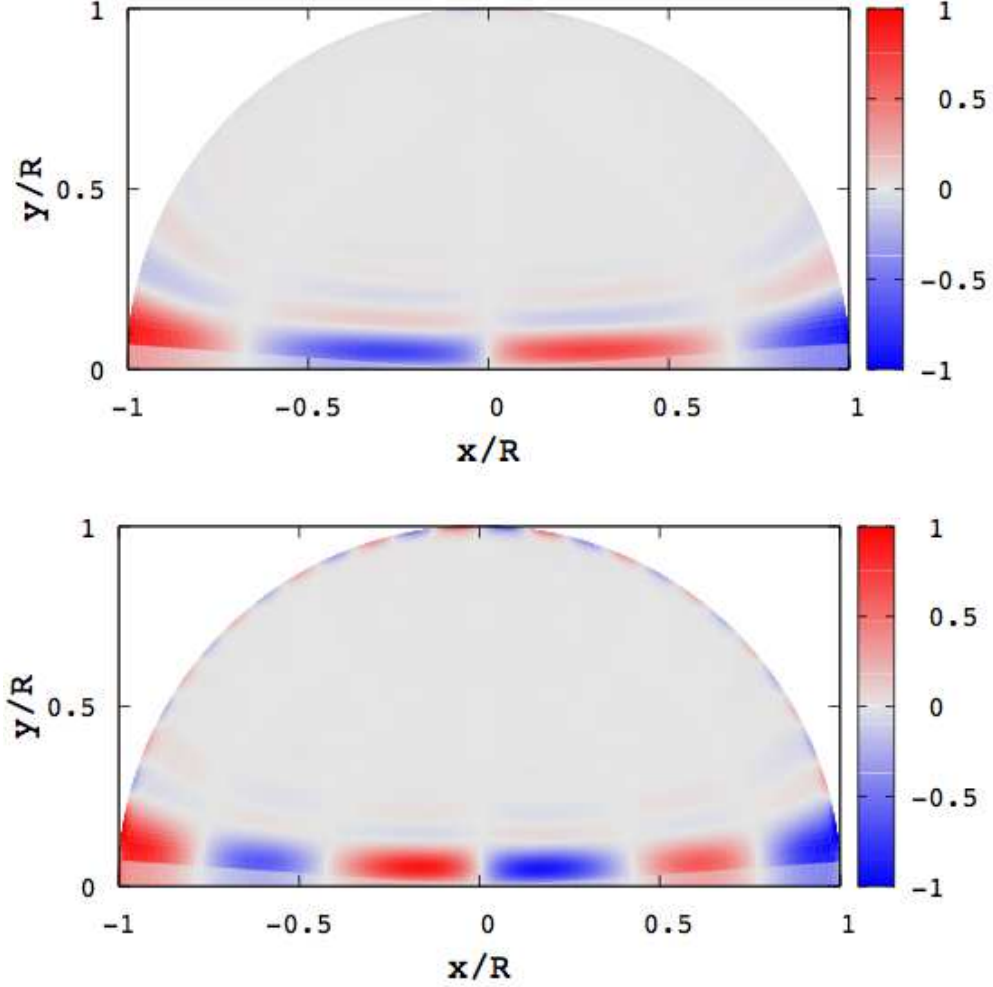


Fig. 7.— Same as Figure 6 but for the modes belonging to the mode sequences O_1 (top panel) and O_2 (bottom panel) in Figure 1, where the modes shown have the least number of radial nodes of $T_{l'_1}$ in each of the mode sequence. The oscillation frequency $\bar{\omega}$ is 0.2235 (top panel) and 0.3720 (bottom panel).

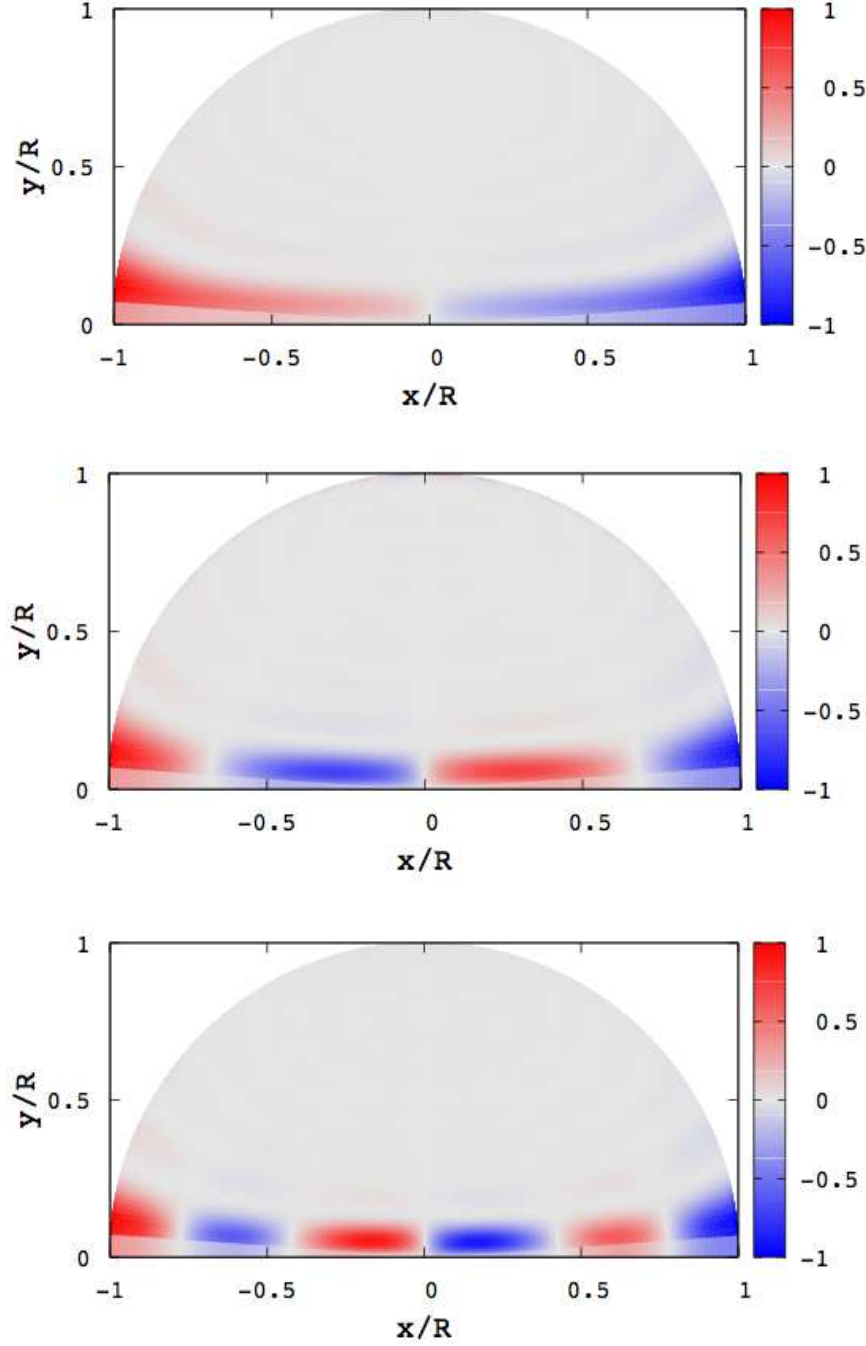


Fig. 8.— Same as Figure 7 but for the modes, from top to bottom panels, belonging to the mode sequences O_0 , O_1 , and O_2 in Figure 4, where the modes have the least number of radial nodes of $T_{l'}$ in each of the mode sequences. Here, the modes are calculated by treating the entire interior as a fluid.

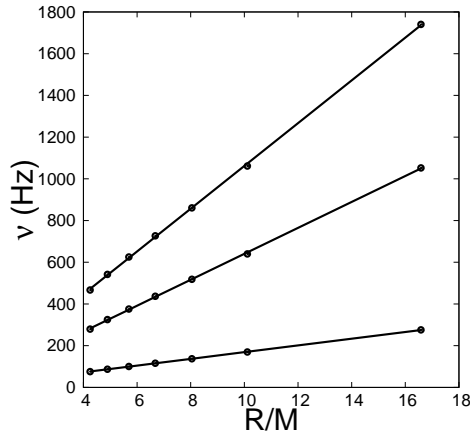


Fig. 9.— Frequencies ν of the axisymmetric toroidal modes of the neutron star models in Table 1 versus the ratio $z \equiv R/M$ for $B_S = 10^{16}$ G, where the modes, from bottom to top, belong to the mode sequences O_0 , O_1 , and O_2 , respectively. Note that the modes with the least number of radial nodes of T_{l_1} are plotted. Also shown are the lines given by the fitting formula (32), where the coefficients in the formula are determined by applying the least-square fit to the frequencies of the mode.

Using the fitting formula (32), we may extrapolate the frequency of the modes to the case of weak magnetic fields. In Figure 10, we plot the frequency $\nu(z, y)$ as a function of z for $y = 0.2$ (solid lines) and $y = 0.1$ (dashed lines). For example, the QPO frequencies observationally detected for SGR 1806-20 are 16.9, 18, 21.4, 30, 36.8, 59.0, 61.3, 92.5, 116.3, 150, and 626 Hz (Israel et al 2005; Strohmayer & Watts 2006; Hambaryan et al 2011). If we assume $y \sim 0.2$ and $z \sim 5$, the frequencies ~ 20 , ~ 60 , and ~ 110 Hz may be reproduced by the formula, but the frequencies around ~ 30 Hz and ~ 92 Hz may not. On the other hand, if we assume $y \sim 0.1$ and $z \sim 15$, the formula can explain the frequencies ~ 30 , ~ 90 , and ~ 150 , but the QPOs of ~ 20 Hz and ~ 60 Hz cannot be fitted by the extrapolation formula. This suggests that it is difficult to explain all the observed QPO frequencies in terms of the toroidal normal modes alone, computed in this paper. For SGR 1900+14, the QPO frequencies are ~ 28 , 53.5, 84, and 155 Hz (Strohmayer & Watts 2005), and these frequencies, except for 53.5 Hz, may be fitted by the formula (32) if we assume $y \sim 0.1$ and $z \sim 14$, suggesting SGR 1900+14 is a low mass neutron star having $\sim 0.7M_{\odot}$ ¹. However, it is also difficult to expect that all the detected QPOs are interpreted in terms of axisymmetric toroidal normal modes alone. It is therefore fair to say that the estimations for the values of y and z given above should be regarded as inconclusive.

To explain the low frequency QPOs having $\nu \lesssim 20$ Hz in terms of the toroidal normal modes, we probably need to assume a weak field B_s of order of 10^{15} G. But, if this is the case, we have a difficulty in explaining high frequency QPOs as high as $\nu \sim 626$ Hz using the toroidal normal modes.

¹Using the EOS APR, Colaiuda & Kokkotas (2011) have estimated a mass $M = 1.4M_{\odot}$, a radius $R = 11.57$ km and a magnetic field $B = 4.25 \times 10^{15}$ G for SGR 1900+14. They have identified the three QPO frequencies 28, 53, 84 Hz as discrete Alfvén modes.

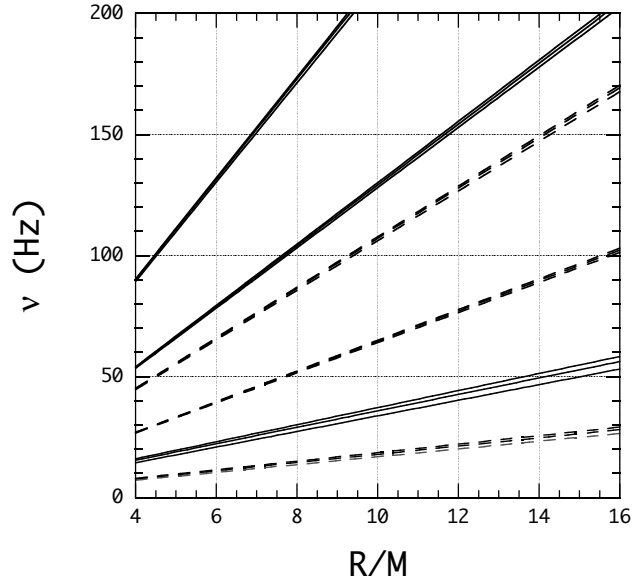


Fig. 10.— Frequencies ν of the first three toroidal modes in each of the mode sequences O_0 , O_1 , and O_2 versus the ratio $z \equiv R/M$ for $y \equiv B_s/(10^{16} \text{ G}) = 0.2$ (solid lines) and $y = 0.1$ (dashed lines).

6. Conclusion

In this paper we have calculated axisymmetric toroidal modes of magnetized relativistic neutron stars with a solid crust, where the interior of the star is assumed to be threaded by a poloidal magnetic field that is continuous at the surface with an outside dipole field. We have obtained axisymmetric toroidal modes of odd parity as normal modes, just as computed by Lee (2008) in the Newtonian formulation. However, no toroidal modes of even parity are found in the present calculation, and the reason for this is not yet well understood. The frequency of the modes is proportional to the magnetic field strength $B_S = \mu_b/R^3$ measured at the surface, suggesting that the modes we obtained are discrete Alfvén modes. We have also calculated axisymmetric toroidal modes in the Newton limit, and we obtained almost the same frequency spectra as those in the general relativistic calculation. In this Newton limit, assuming the Ferraro (1954) type poloidal magnetic field, we can reproduce the results by Lee (2008). This suggests that the difference between the frequency spectra obtained in this paper and by Lee (2008) may be attributable to the difference in the configuration of the poloidal magnetic fields assumed.

Assuming strong magnetic fields ranging from $B_S \sim 5 \times 10^{15}$ G to 10^{16} G, we calculate axisymmetric toroidal modes for neutron stars of different masses. From the frequency spectra thus computed, we find that the frequency is almost exactly proportional to B_S and is well represented by a linear function of R/M for a given value of B_S . This makes it possible to derive a fitting formula for the frequency of the toroidal modes as a function of R/M and B_S . Using thus derived fitting formula, we have tried to determine values of the parameters R/M and B_S such that the toroidal modes can explain the detected QPOs. Although the toroidal mode frequencies for $B_S \sim 10^{15}$ G are in the observed QPO frequency range, we find it difficult to reproduce all the QPO frequencies in terms of the toroidal normal modes alone. This difficulty may suggest that besides the toroidal normal modes we

need different classes of oscillation modes for the QPOs.

As a test of the numerical method we use, taking the expansion length $j_{\max} = 1$ and treating the entire interior as a fluid, we calculated toroidal oscillations and found discrete magnetic modes similar to those obtained by Sotani et al. (2006). The toroidal modes of odd parity in our calculation correspond to the case of $l = 2$ in Sotani et al. (2006). Comparing the frequencies for the model APR+DH14 in Sotani et al (2006) with those for our NS14 model, we found that the frequencies in the two models agree.

In this paper, we reported our finding of discrete toroidal modes of magnetized stars with a poloidal field. This finding seems inconsistent with the results obtained by time-dependent numerical simulations, when most of the simulations suggest only the existence of quasi-periodic oscillations (QPOs) associated with the continua in the frequency spectrum (e.g., Cerdá-Durán et al. 2009; Gabler et al. 2011, 2012, 2013). However, none of the time-dependent numerical simulations could be a mathematical proof of the non-existence of discrete toroidal modes in the magnetized star. We may expect that QPOs associated with continuous frequency spectra and discrete toroidal modes could coexist (e.g., Goedbloed & Poedts 2004). Since our finding is based on the numerical method of a finite precision, we need a mathematically more rigorous proof concerning the existence of discrete toroidal modes in the magnetized stars with a poloidal field.

The present analysis is a part of our study of the oscillations of magnetized relativistic neutron stars. Even for a pure poloidal magnetic field, it is difficult to determine frequency spectra of non-axisymmetric toroidal modes and those of axisymmetric and non-axisymmetric spheroidal modes. We note that the stability of a magnetic field configuration is another difficult problem. It is well known that a purely poloidal magnetic field is unstable and the energy of the field is dissipated quickly, that is, for several ten milliseconds (e.g., Lasky et al. 2011; Ciolfi & Rezzolla 2012), although stellar rotation may

weaken the instability of a poloidal magnetic field as suggested by Lander & Jones (2010). On the other hand, Kiuchi & Yoshida (2008) has calculated equilibrium configurations of rotating relativistic stars having a purely toroidal magnetic field, expecting that some neutron stars have a magnetic field whose toroidal components are much stronger than poloidal ones. But, it was also suggested that purely toroidal magnetic fields are unstable (e.g., Goossens 1979). It is thus anticipated that a mixed poloidal and toroidal magnetic field configuration such as a twisted-torus magnetic field (e.g., Braithwaite & Spruit 2004; Yoshida, Yoshida & Eriguchi 2006; Ciolfi et al. 2009) can be stable, that is, such a magnetic field configuration can last stably for a long time. If this is the case, it will be important to investigate the oscillation modes of stars threaded by both toroidal and poloidal magnetic fields. As suggested by Colaiuda & Kokkotas (2012), however, the presence of a toroidal field component can significantly change the properties of the oscillation modes of magnetized neutron stars. In the presence of both poloidal and toroidal field components, toroidal and spheroidal modes are coupled, which inevitably makes the frequency spectra complex.

As an important physical property inherent to cold neutron stars, we need to consider the effects of superfluidity and superconductivity of neutrons and protons on the oscillation modes. It is believed that neutrons become a superfluid both in the inner crust and in the fluid core while protons can be superconducting in the core. For example, if the fluid core is a type I superconductor, magnetic fields will be expelled from the core region, because of Meissner effect, and hence confined to the solid crust (e.g., Colaiuda et al 2008; Sotani et al 2008). In this case, we only have to consider oscillations of a magnetized crust so long as toroidal modes are concerned, and we have toroidal crust modes modified by a magnetic field. Note that spheroidal oscillations can be propagative both in the magnetic crust and in the non-magnetic fluid core. However, a recent analysis of the spectrum of timing noise for SGR 1806-20 and SGR 1900+14 has suggested that the core region is a type II superconductor (Arras, Cumming & Thompson 2004). If this is the case, the fluid core can

be threaded by a magnetic field and hence the frequency spectra of toroidal modes will be affected by the superconductivity in the core (e.g., Colaiuda et al. 2008; Sotani et al. 2008).

A. Oscillation equations for relativistic magnetized neutron stars

The oscillation equations for axisymmetric toroidal modes in the solid crust are given by

$$r \frac{d}{dr} \mathbf{t} = -\frac{1}{2} \frac{d \ln a_1}{d \ln r} \mathbf{T}_A \mathbf{t} + \pi e^\Lambda \mathbf{T}_B \mathbf{W}, \quad (\text{A1})$$

$$r \frac{d}{dr} \mathbf{W} = -\frac{e^\Lambda}{\beta} \mathbf{K}_A \mathbf{t} - e^\Lambda \mathbf{K}_B \mathbf{W}, \quad (\text{A2})$$

and those in the fluid regions by

$$r \frac{d}{dr} \mathbf{t} = -\frac{1}{2} \frac{d \ln a_1}{d \ln r} \mathbf{T}_C \mathbf{t} + \pi e^\Lambda \mathbf{T}_D \mathbf{h}, \quad (\text{A3})$$

$$r \frac{d}{dr} \mathbf{h} = -e^\Lambda \mathbf{K}_C \mathbf{t} - e^\Lambda \mathbf{K}_D \mathbf{h}, \quad (\text{A4})$$

where the vectors \mathbf{W} and \mathbf{h} are defined, using the vector variables $\mathbf{t} = (T_{l'_j})$ and $\mathbf{b} = (b_{l_j})$, as

$$\mathbf{W} = \frac{\alpha}{\beta} e^{-\Lambda} \mathbf{C}_0 r \frac{d}{dr} \mathbf{t} + \mathbf{Q}_0 \mathbf{C}_1 \mathbf{h}, \quad (\text{A5})$$

$$\mathbf{h} = \frac{r^3}{\sqrt{\pi a_1}} \mathbf{b}. \quad (\text{A6})$$

Here, the matrices in the differential equations are defined by

$$\mathbf{T}_A = \mathbf{M}^{-1} \mathbf{S}_1, \quad (\text{A7})$$

$$\mathbf{T}_B = \mathbf{M}^{-1} \mathbf{C}_1 (\mathbf{Q}_0 \mathbf{C}_1)^{-1}, \quad (\text{A8})$$

$$\mathbf{T}_C = (\mathbf{Q}_1 \mathbf{C}_0)^{-1} \mathbf{S}_1, \quad (\text{A9})$$

$$\mathbf{T}_D = (\mathbf{Q}_1 \mathbf{C}_0)^{-1} \mathbf{C}_1, \quad (\text{A10})$$

$$\begin{aligned} \mathbf{K}_A = e^{-2\Phi} V c_1 \bar{\omega}^2 \left[\left(1 + \frac{p}{\rho} + \frac{p\beta}{\rho\pi} \eta \right) \mathbf{C}_0 + \frac{p\beta}{\rho\pi} (1 - \eta) \mathbf{Q}_0 \mathbf{Q}_1 \mathbf{C}_0 \right] \\ + \alpha (2\mathbf{C}_0 - \mathbf{C}_0 \mathbf{\Lambda}_1) + \alpha \eta \mathbf{S}_A \mathbf{T}_A, \end{aligned} \quad (\text{A11})$$

$$\mathbf{K}_B = e^{-\Lambda} \left(r \frac{d\Phi}{dr} + 2 \frac{d \ln a_1}{d \ln r} - 1 \right) \mathbf{I} + \frac{1}{2} e^{-\Lambda} \frac{d \ln a_1}{d \ln r} \left(\mathbf{S}_B - \frac{\pi\alpha}{\beta} \mathbf{S}_A \mathbf{T}_B \right), \quad (\text{A12})$$

$$\begin{aligned} \mathbf{K}_C = \frac{e^{-2\Phi} V c_1 \bar{\omega}^2}{\beta} \left[\left(1 + \frac{p}{\rho} + \frac{p\beta}{\rho\pi} \eta \right) (\mathbf{Q}_0 \mathbf{C}_1)^{-1} \mathbf{C}_0 \right. \\ \left. + \frac{p\beta}{\rho\pi} (1 - \eta) (\mathbf{Q}_0 \mathbf{C}_1)^{-1} \mathbf{Q}_0 \mathbf{Q}_1 \mathbf{C}_0 \right], \end{aligned} \quad (\text{A13})$$

$$\mathbf{K}_D = e^{-\Lambda} \left(r \frac{d\Phi}{dr} + 2 \frac{d \ln a_1}{d \ln r} - 1 \right) \mathbf{I} + \frac{1}{2} e^{-\Lambda} \frac{d \ln a_1}{d \ln r} (\mathbf{Q}_0 \mathbf{C}_1)^{-1} \mathbf{S}_0, \quad (\text{A14})$$

$$\mathbf{S}_A = \mathbf{S}_0 (\mathbf{Q}_0 \mathbf{C}_1)^{-1} \mathbf{C}_0, \quad (\text{A15})$$

$$\mathbf{S}_B = \mathbf{S}_0 (\mathbf{Q}_0 \mathbf{C}_1)^{-1}, \quad (\text{A16})$$

$$\mathbf{S}_0 = \mathbf{\Lambda}_0 - \mathbf{Q}_0 \mathbf{Q}_1 \mathbf{\Lambda}_0 - 2\mathbf{Q}_0 \mathbf{C}_1, \quad (\text{A17})$$

$$\mathbf{S}_1 = \mathbf{\Lambda}_1 - \mathbf{Q}_1 \mathbf{Q}_0 \mathbf{\Lambda}_1 + 2\mathbf{Q}_1 \mathbf{C}_0, \quad (\text{A18})$$

$$\mathbf{M} = \mathbf{Q}_1 \mathbf{C}_0 + \frac{\pi\alpha}{\beta} \mathbf{C}_1 (\mathbf{Q}_0 \mathbf{C}_1)^{-1} \mathbf{C}_0, \quad (\text{A19})$$

\mathbf{I} is the unit matrix, and

$$\bar{\omega} = \frac{\omega}{\sqrt{M/R^3}}, \quad V = \frac{\rho g r}{p}, \quad g = \frac{M_r}{r^2}, \quad c_1 = \frac{(r/R)^3}{M_r/M}, \quad \alpha = \frac{\mu}{p}, \quad \beta = \frac{a_1^2/r^4}{p}, \quad (\text{A20})$$

where M and R are the gravitational mass and the radius of the star, respectively. Non-zero elements of the matrices \mathbf{C}_0 , \mathbf{C}_1 , \mathbf{Q}_0 , \mathbf{Q}_1 , $\mathbf{\Lambda}_0$, $\mathbf{\Lambda}_1$ are

$$\begin{aligned}
(\mathbf{C}_0)_{jj} &= -(l_j + 2) J_{l_j+1}^m, & (\mathbf{C}_0)_{j+1,j} &= (l_j + 1) J_{l_j+2}^m, \\
(\mathbf{C}_1)_{jj} &= l_j J_{l_j+1}^m, & (\mathbf{C}_1)_{j,j+1} &= -(l_j + 3) J_{l_j+2}^m, \\
(\mathbf{Q}_0)_{jj} &= J_{l_j+1}^m, & (\mathbf{Q}_0)_{j+1,j} &= J_{l_j+2}^m, \\
(\mathbf{Q}_1)_{jj} &= J_{l_j+1}^m, & (\mathbf{Q}_1)_{j,j+1} &= J_{l_j+2}^m, \\
(\mathbf{\Lambda}_0)_{jj} &= l_j (l_j + 1), & (\mathbf{\Lambda}_1)_{jj} &= (l_j + 1) (l_j + 2)
\end{aligned} \tag{A21}$$

for even modes, and

$$\begin{aligned}
(\mathbf{C}_0)_{jj} &= l_j J_{l_j+1}^m, & (\mathbf{C}_0)_{j,j+1} &= -(l_j + 3) J_{l_j+2}^m, \\
(\mathbf{C}_1)_{jj} &= -(l_j + 2) J_{l_j+1}^m, & (\mathbf{C}_1)_{j+1,j} &= (l_j + 1) J_{l_j+2}^m, \\
(\mathbf{Q}_0)_{jj} &= J_{l_j+1}^m, & (\mathbf{Q}_0)_{j,j+1} &= J_{l_j+2}^m, \\
(\mathbf{Q}_1)_{jj} &= J_{l_j+1}^m, & (\mathbf{Q}_1)_{j+1,j} &= J_{l_j+2}^m, \\
(\mathbf{\Lambda}_0)_{jj} &= (l_j + 1) (l_j + 2) & (\mathbf{\Lambda}_1)_{jj} &= l_j (l_j + 1),
\end{aligned} \tag{A22}$$

for odd modes, where

$$J_l^m = \sqrt{\frac{l^2 - m^2}{4l^2 - 1}}. \tag{A23}$$

Table 3: The coefficients c_0 and c_1 for the linear interpolation formulae for DH equations of state.

	c_1	c_0
O_0	16.123	7.797
	16.975	9.614
	17.619	9.877
O_1	62.183	18.543
	62.801	17.843
	63.337	16.988
O_2	102.513	36.627
	103.579	35.997
	104.339	34.316

REFERENCES

- Arras P., Cumming A., Thompson C., 2004, *ApJ*, 608, L49
- Akmal A., Pandharipande V. R., Ravenhall D. G., 1998, *Phys. Rev. C*, 58, 1804
- Baym G., Pethick C., Sutherland P., 1971, *ApJ*, 170, 299
- Braithwaite J., Spruit H. C., 2004, *Nature*, 431, 819
- Cerdá-Durán P., Stergioulas N., Font J. A., 2009, *MNRAS*, 397, 1607
- Ciolfi R., Ferrari V., Gualtieri L., Pons J. A., 2009, *MNRAS*, 397, 913
- Ciolfi R., Rezzolla L., 2012, *ApJ*, 760, 1
- Colaiuda A., Ferrari V., Gualtieri L., Pons J. A., 2008, *MNRAS*, 385, 2080
- Colaiuda A., Kokkotas K. D., 2011, *MNRAS*, 414, 3014
- Colaiuda A., Kokkotas K. D., 2012, *MNRAS*, 423, 811
- Douchin F., Haensel P., 2001, *A&A*, 380, 151
- Duncan R. C., Thompson C., 1992, *ApJ*, 392, L9
- Ferraro V. C. A., 1954, *ApJ*, 119, 407
- Gabler M., Cerdá-Durán P., Font J. A., Müller E., Stergioulas N., 2011, *MNRAS*, 410, L37
- Gabler M., Cerdá-Durán P., Stergioulas N., Font J. A., Müller E., 2012, *MNRAS*, 421, 2054
- Gabler M., Cerdá-Durán P., Font J. A., Müller E., Stergioulas N., 2013, *astrophysics*,
arXiv:1208.6443v2
- Glampedakis K., Samuelsson L., Andersson N., 2006, *MNRAS*, 371, L74

- Goedbloed H., Poedts S., 2004, *Principles of Magnetohydrodynamics with Applications to Laboratory and Astrophysical Plasma*, Cambridge University Press, Cambridge
- Goosens M., 1979, *A&A*, 123, 147
- Hambaryan V., Neuhauser R., Kokkotas K. D., 2011, *A&A*, 528, A45
- Israel G., Belloni T., Stella L., Rephaeli Y., Gruber D. E., Casella P., Dall’Osso S., Rea N., Persic M., Rothschild R. E., 2005, *ApJ*, 628, L53
- Kiuchi K., Yoshida S., 2008, *astrophysics*, arXiv:0802.2983v1
- Konno K., Obata T., Kojima Y., 1999, *A&A*, 352, 211
- Lander S. K., Jones D. I., 2010, *astrophysics*, arXiv:1010.0614v2
- Lasky P. D., Zink B., Kokkotas K. D., Glampedakis K., 2011, *ApJ*, 735, L20
- Lee U., 2005, *MNRAS*, 357, 97
- Lee U., 2007, *MNRAS*, 374, 1015
- Lee U., 2008, *MNRAS*, 385, 2069
- Levin Y., 2007, *MNRAS*, 377, 159
- Messios N., Papadopoulos D. B., Stergioulas N., 2001, *MNRAS*, 328, 1161
- Piro A. L., 2005, *ApJ*, 634, L153
- Saio H., Gautschi A., 2004, *MNRAS*, 350, 485
- Schumaker B. L., Thorne K. S., 1983, *MNRAS*, 203, 457
- Sotani H., Kokkotas K. D., Stergioulas N., Vavoulidis M., 2006, *astrophysics*, arXiv:0611666v1

- Sotani H., Kokkotas K. D., Stergioulas N., 2007, MNRAS, 375, 261
- Sotani H., Kokkotas K. D., Stergioulas N., 2008, MNRAS, 385, L5
- Sotani H., Colaiuda A., Kokkotas K. D., 2008, MNRAS, 385, 2161
- Strohmayer T. E., Watts A. L., 2005, ApJ, 632, L111
- Strohmayer T. E., Watts A. L., 2006, ApJ, 653, 593
- Strohmayer T.E. Ogata S., Iyetomi H., Ichimaru S., Van Horn H. M., 1991, ApJ, 375, 679
- Thompson C., Duncan R. C., 1995, MNRAS, 275, 255
- Unno, W., Osaki, Y., Ando, H., Saio, H., Shibahashi, H., 1989, Nonradial Oscillations of Stars, 2nd Ed, University of Tokyo Press, Tokyo
- Van Hoven M., Levin Y., 2011, MNRAS, 410, 1036
- Van Hoven M., Levin Y., 2012, MNRAS, 420, 3035
- Watts A. L., Strohmayer T. E., 2006, ApJ, 637, L117
- Yoshida S., Yoshida S., Eriguchi Y., 2006, ApJ, 651, 462